CNRS
Centre National de la Recherche Scientifique

INFN
Istituto Nazionale di Fisica Nucleare

AdV - Stray Light Control: Requirements for wide-angle scattering in the arm cavity

VIR-0055A-13

A. Chiummo[1*], R. Day[1], and J. Marque[1]

[1] *EGO - European Gravitational Observatory*

Date: February 13, 2013

[*] *corresponding author:* antonino.chiummo@ego-gw.it

VIRGO* A joint CNRS-INFN Project - EGO* the site of the VIRGO project
Via E. Amaldi, I-56021 S. Stefano a Macerata - Cascina (Pisa)
Secretariat: Telephone (39) 050 752 521 * FAX (39) 050 752 550 * Email: ego@ego-gw.it

Contents

Introduction 2

1 Noise projection for path (2) 3

2 Coupling ratio for wide-angle scattered light 3
2.1 Method1: FFT and BRDF combined calculation . . . 4
2.1.1 BRDF-based calculation . . . 4
2.1.2 FFT-based calculation . . . 5
2.2 Method2: BRDF and Reciprocity Theorem calculation . . . 6

3 Requirements for exposed surfaces in the Test Mass towers 6
3.1 Scattering surface . . . 8
3.2 Reflective surface . . . 8

Conclusions 11

Aknowledgments 11

A Limit between small and wide angle scattering 12

References 15

Introduction

Three kinds of stray light coupling paths have been identified for the test masses of AdV and its surroundings (see fig. 1):

1. small-angle scattering from the farthest mirror, wide-angle scattering from the baffle, small-angle scattering from the farthest mirror.
2. wide-angle scattering from nearest mirror, wide-angle scattering from baffles or other surfaces, wide-angle scattering from the nearest mirror.
3. wide-angle scattering from the nearest mirror, wide-angle scattering from the cryotrap walls, small-angle scattering from the farthest mirror (and viceversa);
   wide-angle scattering from the nearest mirror, wide-angle scattering from the cryotrap walls, wide-angle scattering from the nearest mirror.

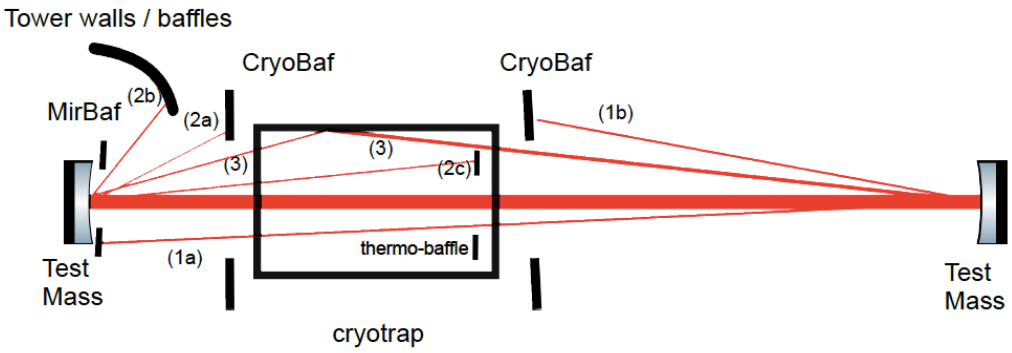

Figure 1: Re-coupling paths for scattered light (lengths not in scale). In this document we focus on path (2). Path (1) was studied in ref.[3, 4] while ref.[5] made calculations about path (3).

The limit between small and wide angle scattering of the mirror can be defined as the angle at which the quantity of scattering due to the roughness of the mirror is equal to the quantity of scattering due to point defects (assuming the distribution of point defect scattering is Lambertian). Indeed, it has been demonstrated experimentally that the quantity of light scattered at large angle from the test masses of the first generation GW interferometer is largely dominated by point defects over the micro-roughness contribution [1].
The limit between small and wide angle scattering of the mirror is then 0.7 degrees or 12 mrad, from the extrapolation of expected PSD, while **an upper limit is set at 3 degrees or 52 mrad**, when we consider available data in literature [2] (see annex A for details).

The study of what is labelled by path (1) was carried out in [3, 4].
Analytical calculations were performed by J-Y. Vinet [5] for the case (3).
In this document we address the issues related to path (2). Chapter 1 describes the general model for calculating the displacement noise of baffles for path (2). Two different methods to derive the coupling of this scattered light into the ITF mode are detailed in Chapter 2: we study in particular the case of the thermo-baffle of the cryotrap [6], a surface that is likely to be impossible to hide completely from the test mass view. Chapter 3 gives the final requirements for wide angle scattering around the test masses of the arm cavities. Further requirements are given for the reflection from surfaces such as metallic mountings, inside the towers of the test masses.

1 Noise projection for path (2)

Both in [3, 4], the projection h_{xxBaf} of the baffle displacement noise to the AdV strain sensitivity was computed in two steps:
a) FFT simulations (use of FOG [7]) to derive the fraction of the power impinging onto the baffle that couples to the main mode of the ITF;

b) estimation of the transfer function from the baffle displacement noise to the AdV strain sensitivity (use of Optickle, [8]), namely:

$$h_{Baf} = \frac{TF_{df/x_{Baf}}}{TF_{df/DARM}} \frac{1}{L_{arm}} |c_{xxBaf}| \times \tilde{x}_{Baf} \sim \frac{1}{L_{arm}} |c_{xxBaf}| \times \tilde{x}_{Baf} \tag{1.1}$$

where $|c_{xxBaf}|^2$ is the fraction of the power in the arm cavity that couples with the main mode after scattering from the baffle *xxBaf*. $TF_{df/x_{Baf}}$ is the transfer function from the baffle displacement noise to the dark fringe photodiode for a baffle that couples all the arm cavity power to the main mode, $TF_{df/DARM}$ is the transfer function from the differential-arm displacement to the dark-fringe photodiode, and $\tilde{x}_{Baf}$ is the displacement of the baffle.
While the second step can be kept, the path (2) involves scattering calculations at large angles, so that FFT propagations are no more suited.
One option is to adapt this method by replacing the FFT simulation with calculations based upon the BRDF of concerned surfaces, in order to get the power that is scattered by the test mass after the scattering from a baffle along path (2). Then, this power has to be multiplied by a suitable coefficient, $|c_{xxBaf}|^2$, to obtain the amount of power scattered to the main mode of the arm cavity, per Watt of arm cavity power P_{arm}.
This coupling coefficient, $|c_{xxBaf}|^2$, is the power of scattered light from the test mass and the baffle - through the path (2) - onto the main arm-cavity mode, divided by the arm-cavity power:

$$|c_{xxBaf}|^2 = P_{scat}/P_{00} \; |c_{scat}|^2 \tag{1.2}$$

with c_{scat} the projection of the scattered field onto the cavity mode:

$$|c_{scat}|^2 = \left| \frac{\int E_{00}^* E_{scat} dxdy}{\sqrt{\int |E_{00}|^2 dxdy \; \int |E_{scat}|^2 dxdy}} \right|^2 \tag{1.3}$$

where E_{00} is the amplitude of the main arm-cavity mode, and E_{scat} is the scattered field from the test mass, at the end of path (2), carrying a power P_{scat}.
In the next section, the coupling efficiency for the cryo-trap thermo-baffle, $|c_{TBaf}|^2$, will be derived in two different ways.

2 Coupling ratio for wide-angle scattered light

In this section, we will calculate the coupling ratio $|c_{TBaf}|^2$ in the case of the thermo-baffle with two different models for cross-check purpose.

2.1 Method1: FFT and BRDF combined calculation

2.1.1 BRDF-based calculation

The BRDF of a scattering surface hit by a power P_i, scattering an amount of power P_s to an angle θ_s within a solid angle Ω_s, can be written as [10]:

$$BRDF(\theta_s) = \frac{dP_s/d\Omega_s}{P_i \ \cos(\theta_s)} \sim \frac{P_s/\Omega_s}{P_i \ \cos(\theta_s)} \tag{2.1}$$

Given the fact that θ_s is small in the case of Thermo-baffle, an upper limit for the scattered power from a surface can be estimated by means of its BRDF as:

$$P_s(\theta_s) = P_i \ BRDF(\theta_s) \ \Omega_{sur} \tag{2.2}$$

where Ω_{sur} is the solid angle of the target area as seen from the scattering source.

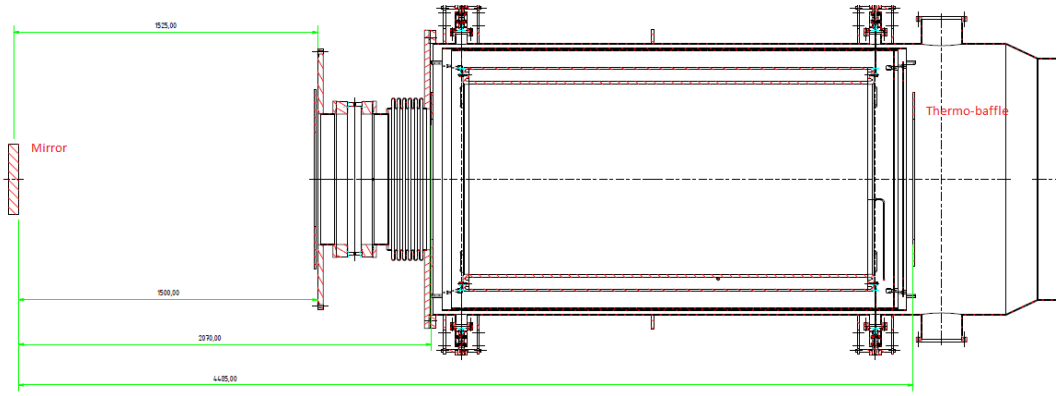

Figure 2: Mechanical layout of the Thermo-baffle and mirror.

Table 1: Parameters for path (2)

TIS^{Mir} wide angle	$10ppm \ W/W$
$BRDF^{Mir}$ wide angle	$TIS^{Mir}/\pi \ sr^{-1}$
Ω_{TBaf}	$2.1 \times 10^{-2} \ sr$
L_{TBaf}	$4.4 \ m$
L_{cav}	$3000 \ m$
TIS^{TBaf}	1
$BRDF^{TBaf}$	$0.3 \ sr^{-1}$
Ω_{Mir}	$5 \times 10^{-3} \ sr$
$S_{Mir} = \pi r_{mir}^2$	$9.6 \times 10^{-2} \ m^2$
$\lvert c_{scat}\rvert^2$	$3 \times 10^{-11} \ W/W$

In order to estimate $|c_{TBaf}|^2$ for the thermo-baffle of the cryo-trap, we apply first the formula 2.2 to get the total power scattered from the test mass towards the thermo-baffle. Then, we compute the fraction of this power that is backscattered to the test mass due to the baffle scattering (given the geometry of the problem, see fig. 2), and hence the fraction of this power that is scattered again off the test mass. This power is not totally in the TEM_{00} mode of the arm cavity, on the contrary only a fraction $|c_{scat}|^2$ is actually carried by the TEM_{00}.
Putting it all together:

$$|c_{TBaf}|^2 = BRDF^{Mir} \ \Omega_{TBaf} \times BRDF^{TBaf} \ \Omega_{Mir} \times TIS^{Mir} \times |c_{scat}|^2 \tag{2.3}$$

where Ω_{Mir} is the solid angle of the test mass as seen from the thermo-baffle, Ω_{TBaf} is the solid angle of the thermo-baffle as seen from the test mass, TIS^{Mir} is the Total Integrated Scattering of the Test Mass, and the parameters listed in tab.1 are assumed.
In the next paragraph we will evaluate the coefficient $|c_{scat}|^2$.

2.1.2 FFT-based calculation

Last step of path (2) process is the wide-angle scattering from the test mass to the main arm-cavity mode. The field originating from wide-angle scattering presents a speckle-like distribution, whose features are related to the illumination pattern on the scattering surface and the propagation distance [9]. We will calculate the upper limit of this coupling coefficient, $|c_{scat}|^2$, thanks to FFT propagation.
The direct simulation of wide-angle scattering is extremely difficult due to the extremely high spatial sampling rate that would be required in the grid representing the field to be propagated. We therefore use the BRDF properties of each diffusing surface in order to estimate the power that will be diffused from the test mass (say the input mirror) in the direction of the opposite mirror (the end mirror). We determine a virtual source at the level of the input mirror representing the light diffused from said mirror. The light scattered from the tower baffles, possible exposed surfaces, and the cryo-trap baffle, and reaching the input mirror will be evenly distributed. Therefore for the virtual source we choose a constant amplitude over the whole surface of the input mirror. As the virtual source represents scattered light, its phase distribution is random. The total power of the virtual source is normalized such that the total power, after propagation, reaching the end mirror is the same as that estimated from the calculations using the BRDF properties of each diffusing surface. Two methods were used for determining the coupling of this virtual source into the cavity mode:

1. The cavity is locked and simulated in the usual way with FOG using an external field source matched to the cavity mode. The TEM_{00} power in the cavity is noted and the microscopic cavity length is frozen. We then converge again to steady state, this time using the intra-cavity virtual source defined previously and determine the TEM_{00} power in the cavity. The ratio of the powers determined in these two simulations gives the coupling coefficient of the diffused light into the cavity mode (see fig. 3(a)).
2. In this much simpler approach we calculate the ratio of TEM_{00} power to total power for the virtual source (see fig. 3(a)). We confirmed numerically that these two approaches were equivalent. As the second approach requires no propagation and numerical convergence it is much faster and so it is the approach we use in the following simulations. We carried out 5000 simulations using each time a different random phase distribution for the virtual source. Due to the random nature of the virtual source phase there is a relatively large distribution in the measured coupling factor.

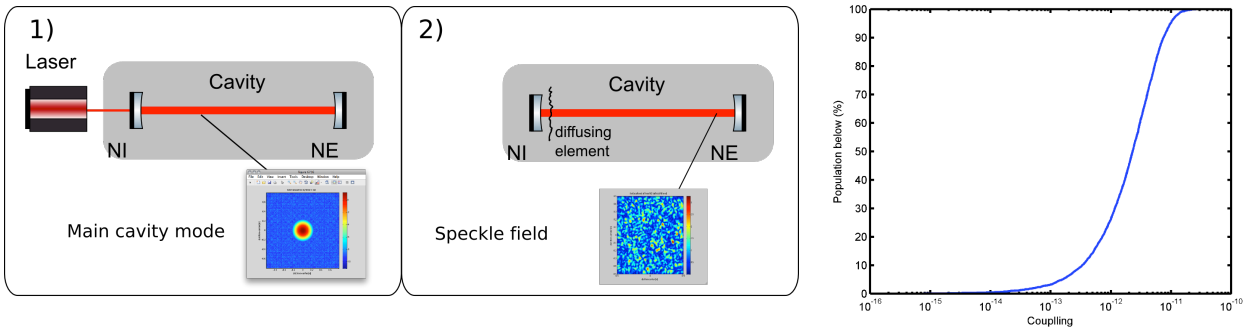

(a) (b)

Figure 3: Fig.(a): Sketch of the setup used for FFT simulation with FOG, to calculate the coupling of "wide-angle" scattered light to the main cavity mode: 1) Simulation to find the cavity main mode; 2) Diffusing element inside the cavity to produce a speckle-like field. Fig.(b): Cumulated distribution of the results for $|c_{scat}|^2$. An upper limit of $|c_{scat}|^2 \lesssim 3 \times 10^{-11}\ W/W$ has been derived from those simulations (5000 runs).

Figure 3(b) shows the proportion of the 5000 simulations for which the coupling factor is below a certain value. We see that almost 100% of the population is below:

$$|c_{scat}|^2 \lesssim 3 \times 10^{-11}\ W/W \tag{2.4}$$

which we may therefore consider as the upper limit.
By using the value for $|c_scat|^2$ found in this subsection, the overall coupling efficiency for the scattering of path (2) of the thermo-baffle can be estimated to be:

$$(\mathbf{1})\mathbf{BRDF} \left\{ \begin{array}{rcl} c_{TBaf}|^2 & = & BRDF^{Mir}\ \Omega_{TBaf} \times BRDF^{TBaf}\ \Omega_{Mir} \times TIS^{Mir} \times |c_{scat}|^2 \\ & \sim & 3 \times 10^{-26}\ W/W \end{array} \right. \tag{2.5}$$

2.2 Method2: BRDF and Reciprocity Theorem calculation

Another approach to compute the recoupled scattered light is used by aLIGO [11]. This approach involves both the BRDF concept and the evaluation of a "cross section" σ for the scattering towards the arm-cavity main mode. The formula to estimate the coupling coefficient with this approach is:

$$|c_{TBaf}|^2 = \frac{I_s}{P_i}\ \sigma \tag{2.6}$$

where I_s is the irradiance of power scattered back from the baffle, a distance L_{Baf} away from the test-mass mirror, at the level of test-mass mirror:

$$I_s = P_{TBaf}\ TIS^{TBaf}\ 1/L^2_{TBaf} \tag{2.7}$$

where $P_{TBaf} = P_i\ BRDF^{mir}\ \Omega_{mir}$ is the power scattered by the test mass that reaches the thermo-baffle. The cross-section for the recombination of a photon coming from a direction θ_s to the arm-cavity main mode, as defined by [12], is:

$$\sigma = \lambda^2\ BRDF^{mir}\ \cos(\theta_s) \tag{2.8}$$

This gives an estimation for the coupling coefficient:

$$(\mathbf{2})\mathbf{Rec.Th.} \left\{ \begin{array}{rcl} |c_{TBaf}|^2 & = & \frac{I_s}{P_i}\ \sigma \\ & = & \frac{P_{TBaf}}{P_i}\ BRDF^{TBaf}\ \pi\ \cos(\theta_s)^2\ \frac{1}{L^2_{TBaf}}\ \lambda^2\ BRDF^{mir} \\ & = & (BRDF^{mir})^2\ \Omega_{TBaf}\ BRDF^{TBaf}\ \pi\ \cos(\theta_s)^2\ \frac{\lambda^2}{L^2_{TBaf}} \\ & \sim & 1.2 \times 10^{-26}\ W/W \end{array} \right. \tag{2.9}$$

where the parameters listed in tab.1 are used, along with $\lambda = 1.064 \mu m$ for the YAG laser. The value 2.9 obtained with this method is roughly ∼2.5 times smaller than the upper limit based on BRDF calculations and projection of the scattered field (2.5).

3 Requirements for exposed surfaces in the Test Mass towers

In [4], we saw that coupling coefficients are acceptable below $10^{-24}\ W/W$ for ground-connected scattering surfaces inside the arm cavities (see also fig.4). Starting from this result, in this section we will derive requirements for both scattering and reflective surfaces inside the test mass towers (see fig. 5).

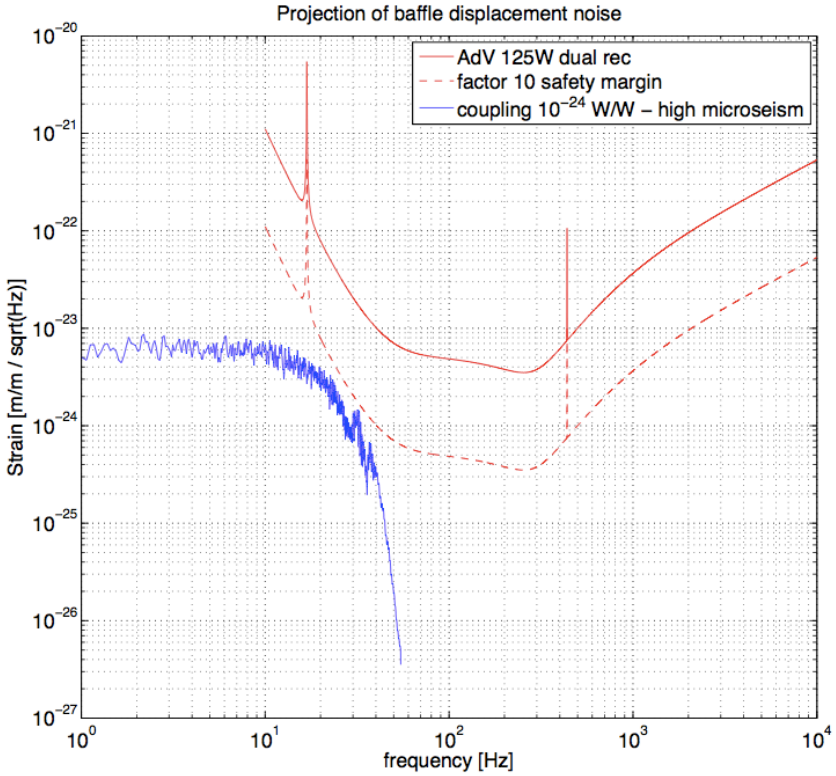

Figure 4: Baffle displacement noise projection on AdV baseline strain sensitivity, for a coupling of scattered light $|c_{xxBaf}|^2 \sim 10^{-24}\ W/W$. The projection is made for the case of high μ-seism (see [4]), and the baffle is assumed to be ground-connected.

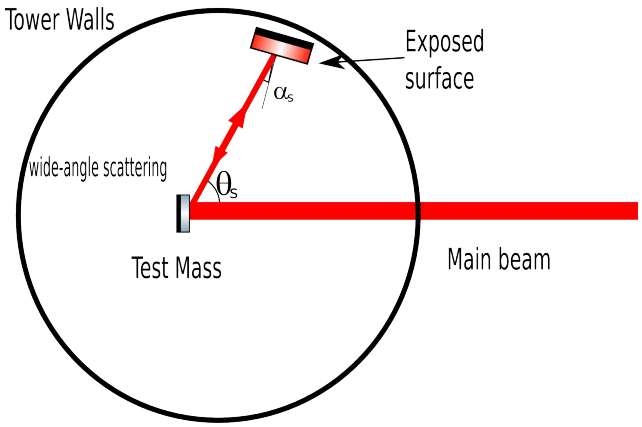

Figure 5: An exposed surface on the tower walls at an angle θ_s from the test mass, tilted by an angle α_s with respect to the line of sight, intercepts some of the power scattered off the test mass, and hence possibly scatters and/or reflects a fraction of this power back towards the test mass. Due to the geometrical constraints of the walls, α_s is generally small ($\cos(\alpha_s) \sim 1$).

3.1 Scattering surface

Let us consider a surface on the tower walls, (i.e. ground-connected and at roughly $d_{sur} \sim 1m$ from the test mass), at an angle θ_s and tilted by an angle $\alpha_s < 10°$ with respect to the line of sight from the test mass, so that $cos(\alpha_s) \sim 1$. Then a requirement can be derived for its area, A_{sur}, once that its BRDF, say $BRDF_{sur}$, is known. By using 2.5, we can write:

$$|c_{sur}|^2 = BRDF^{Mir} \cos(\theta_s)\ \Omega_{sur} \times BRDF^{sur}\ \Omega_{Mir} \times TIS^{Mir} \times |c_{scat}|^2 \lesssim 10^{-24} W/W \tag{3.1}$$

or:

$$A_{sur} < \frac{d_{sur}^4}{BRDF^{sur}\ BRDF^{Mir}\ S_{Mir}\ TIS^{Mir}\ |c_{scat}|^2\ \cos(\theta_s)} \times 10^{-24} W/W \tag{3.2}$$

where S_{Mir} is the area of the test mass. Let us suppose at this point that the surface in question has a square-shape when projected upon a plane perpendicular to the line-of-sight from the test mass. **That means that if such a surface features a $BRDF = 0.3 sr^{-1}$ (Lambertian scatterer), is located within an angle $\theta_s < 10°$ with respect to the Test Mass center, at a distance $d_{sur} \sim 1m$, then it cannot have a side larger than $\mathbf{l_{sur}} \sim 0.19$ m.**

In figure 6, we report the requirements in term of maximum surface area of a ground-connected element with $BRDF = 1 sr^{-1}$ depending on its distance to the mirror and θ_s. It is worth stressing that such a requirement is drawn by considering the safety margin of ten with respect to AdV sensitivity. So a unique Lambertian scattering surface at a distance of 1m from the mirror, with an area of $\sim 400 cm^2$, **already saturates the safety margin**. **This implies that the tower walls must be baffled carefully over almost a solid angle of 2π sr**.
The maximum allowed surface area of a scatterer having a BRDF different than 1 can be deduced from fig. 6 by rescaling linearly the surface with the BRDF (see eq. 3.2). For instance, a baffle diaphragm (with external diameter of 1m, and internal diameter of 0.6m) located at a distance of 1m from the mirror and having a BRDF of 0.01 sr^{-1} is fine since its surface is $\sim 0.5 m^2$ while the maximum surface area for such a baffle is about $\sim 1 m^2$.

3.2 Reflective surface

The same argument used in the previous sub-section can be applied to derive requirements for reflective surfaces inside the towers of the test masses.
Let us consider a flat reflective surface on the tower walls, S_{Refl}, at an angle θ_s and a distance $d_{SRefl} \sim 1m$ from the test mass, for instance. Some of the power that is scattered off the test mass reaches the reflective surface, and hence a fraction of this power is possibly reflected back to the test mass. We will assume that S_{Refl} is almost at a normal angle with respect to the line-of-sight from the test mass so that the reflection off said surface hits the test mass mirror. We can derive a requirement on the largest tolerable area for such a surface.

The power reaching S_{Refl} is reflected back to the test mass, attenuated by the reflectivity of S_{Refl}:

$$P_{SRefl\ (small)} = P_i\ BRDF^{Mir}\ \cos(\theta_s)\ \Omega_{SRefl\ (small)} \times R_S \tag{3.3}$$

where R_S is the (intensity) reflectivity of S_{Refl} and $\Omega_{SRefl\ (small)} = A_{Refl}\ /\ d^2_{SRefl}$ is the solid angle of the reflective surface as seen from the test mass. This power will be scattered once again off the test mass and, as usual, a fraction $|c_{scat}|^2$ (eq.1.3) is assumed to couple with the arm-cavity main mode. The overall coupling efficiency for this process is required to be smaller than $10^{-24} W/W$:

$$|c_{sur(R\ small)}|^2 = \frac{P_{SRefl\ (small)}}{P_i}\ TIS^{Mir} \times |c_{scat}|^2 \lesssim 10^{-24} W/W \tag{3.4}$$

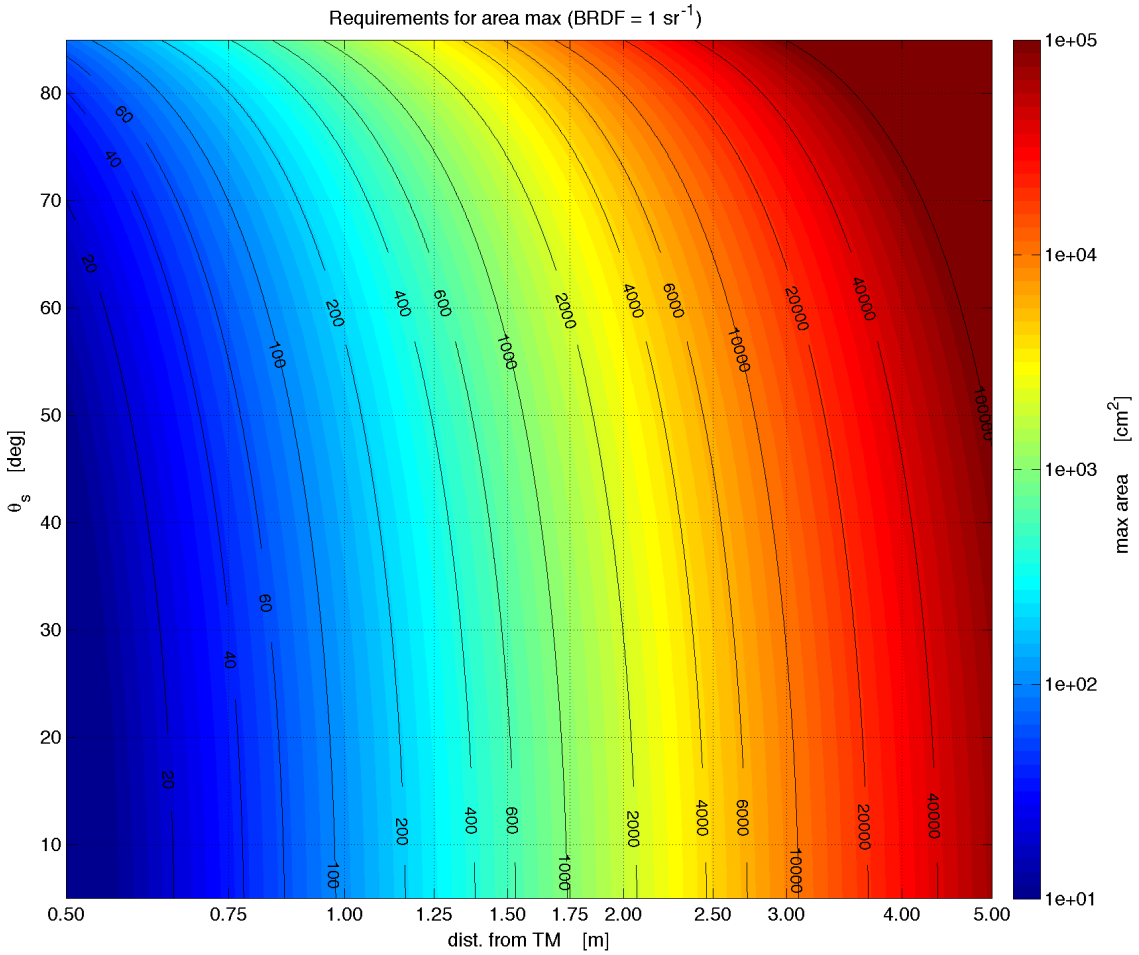

Figure 6: Requirement for the maximum surface area of a scatterer with $BRDF = 1sr^{-1}$, as a function of the distance to the mirror and the angle with respect to the optical axis.

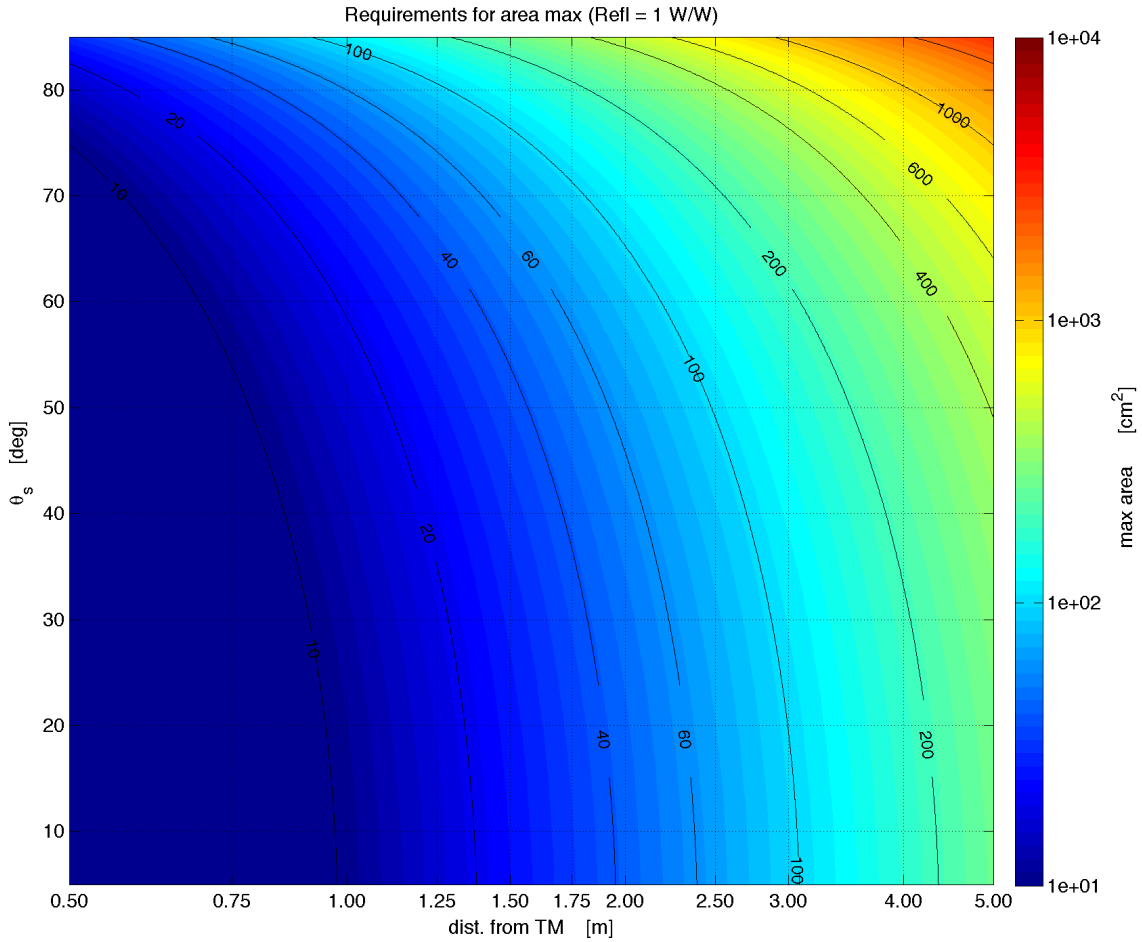

Figure 7: Requirement for the maximum surface area of a reflective surface with $R = 1$, as a function of the distance to the mirror and the angle with respect to the optical axis.

with obvious meaning of the symbols. This result allows us to derive a maximum tolerable surface area:

$$A_{Refl} \lesssim \frac{R_S\ 10^{-24}\ W/W}{(BRDF^{Mir}\ \cos(\theta_s)\ \Omega_{SRefl}\ TIS^{Mir}\ |c_{scat}|^2} = \frac{10^{-24}\ W/W}{\pi\ |c_{scat}|^2}\ \frac{1}{(BRDF^{Mir})^2} \times \frac{d^2_{SRefl}}{R_S\ \cos(\theta_s)} \tag{3.5}$$

In figure 7, we report the requirements in term of maximum surface area of a ground-connected element with $R_S = 1$ depending on its distance to the mirror and θ_s.
Let's assume for instance that a metallic mounting is exposed to the test mass view at an angle of 45 degrees and a distance of 1m, its reflectivity for YAG wavelength being very high, say ~ 1. Then the largest allowable area for such a mounting is $\sim 15cm^2$. It is worth stressing that this value **already saturates the safety margin**, so that it is recommended to have a further safety margin.

Conclusions

We have explored two methods to evaluate the coupling of stray light, originating from the wide-angle (>0.7 degree) scattering of the arm cavity test mass mirrors. The methods are both based on analytical approximations to find the total amount of power scattered at the end of what we termed path (2). Those methods differ in the technique to estimate the amount of such a power that is carried by the arm-cavity TEM_{00} and hence affects AdV sensitivity. While the technique used in LIGO and described in section 2.2 relies onto the analytical calculations made in [11, 12], the one employed in section 2.1 is based upon FFT propagation simulations, and is intended to set an upper limit for the coupling coefficient. Anyway, both the techniques give comparable results (within a factor ~ 3).

We applied this study to the case of the thermo-baffle of the end tower cryotrap, and found that the resulting coupling coefficient is acceptable from the SLC point of view.
We finally derived two general equations (and their relative plots: figures 6 and 7) that define the maximum surface area of a scatterer or a reflector depending on their location with respect to the mirror and depending on their optical property (BRDF and Reflectivity).
One can extract from these two plots the SLC requirements for any ground connected objects located in the surrounding of the test mass mirrors. For instance, we found that a Lambertian scatterer located at 1m from the mirror and close to the optical axis cannot have a surface larger than $400cm^2$.
Moreover, a high-reflective and ground-connected surface (such as possible metallic mounts) can be an issue if its total area is larger than $\sim 0.0011\ m^2$, or a square with a side of ~ 3.3 cm, when this surface is located $\sim 1\ m$ away from the test mass and at an angle of $\sim 15°$.
It is worth stressing that each of those requirements have been derived by taking into account the whole safety margin of ten with respect to the baseline AdV sensitivity, so the SLC subsystem does recommend to keep further margin.

Aknowledgments

The authors wish to acknowledge fruitful discussions with Benjamin Canuel, and Eric Genin.

A Limit between small and wide angle scattering

The expected Power Spectral Density of the core mirrors for AdV has been calculated from the surface maps provided by LMA. We extrapolated this PSD to higher spatial frequencies following the scale law:

$$PSD(\rho) = A\ (\frac{\rho}{\rho_\mu})^b \tag{A.1}$$

where $A = 2.9108\ 10^{-22}\ m^3$, $\rho_\mu = 101.3\ m^{-1}$, and $b = -2.52$ are the parameters of the fit. Available data in literature [2] suggest that the scale law might be less steep, with a power law $\sim \rho^{-1.5}$. In fig.8 we report both the cases of the extrapolation from the available surface maps, and the scale law of reference [2].

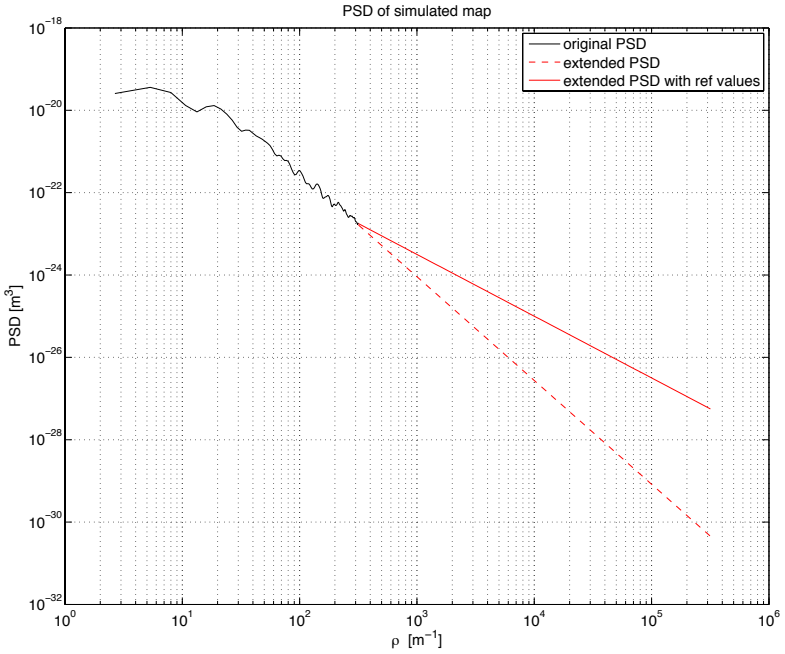

Figure 8: Typical PSD of the phase map of the AdV arm mirrors and its extrapolation to higher spatial frequencies. Solid line refers to the power law found in [2], while the dashed line is the extrapolation from available surface maps of core mirrors.

The BRDF corresponding to the previous PSD can be calculated as follows [10]:

$$BRDF(\theta_s) = \frac{16\ \pi^2}{\lambda^4} \cos(\theta_i)\ \cos(\theta_s)\ Q\ \frac{PSD(\rho)}{2\pi\ \rho} \tag{A.2}$$

where ρ is the spatial frequency, $\theta_s = \arcsin(\rho\lambda)$ is the angle of scattering, θ_i is the angle of incidence, and $Q \sim 1$ is a coefficient accounting for the difference of reflectivity due to the polarization.
The Total Integrated Scattering from the core optics due to the point defects, is expected to be $TIS \sim 10ppm$, so the BRDF for point defects can be assumed to be: $BRDF_{pd} = TIS/\pi \sim 3\ 10^{-6} sr^{-1}$. By looking at figure 9, we can see that this value of $BRDF_{pd}$ is larger than the BRDF for roughness starting at an angle $\theta_s \sim 0.7°$ if we consider the extrapolation of the PSD drawn from the available maps, while this angle becomes $\sim 3°$ when considering the power law found in [2].
Nevertheless, recent measurements [13] performed on core optics at LIGO, show that the actual BRDF's for real mirrors could need a more complex model to be accounted for (see fig. 10).

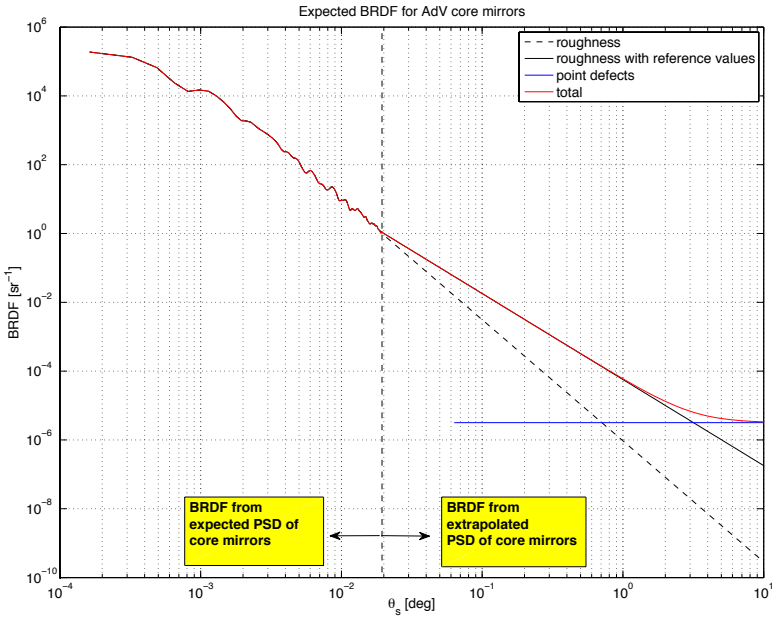

Figure 9: Expected BRDF for AdV core optics. The BRDF contribution from the point defect scattering becomes dominant over the roughness one from angles as small as $\sim 0.7°$ if we consider the extrapolation of the PSD drawn from the available maps (dashed line), while this angle becomes $\sim 3°$ when considering the power law found in [2]. The dashed vertical line at $\theta_s \sim 0.02°$, instead, divides the region of BRDF derived from expected PSD of core mirrors (left), from the one obtained from extrapolated PSD (right).

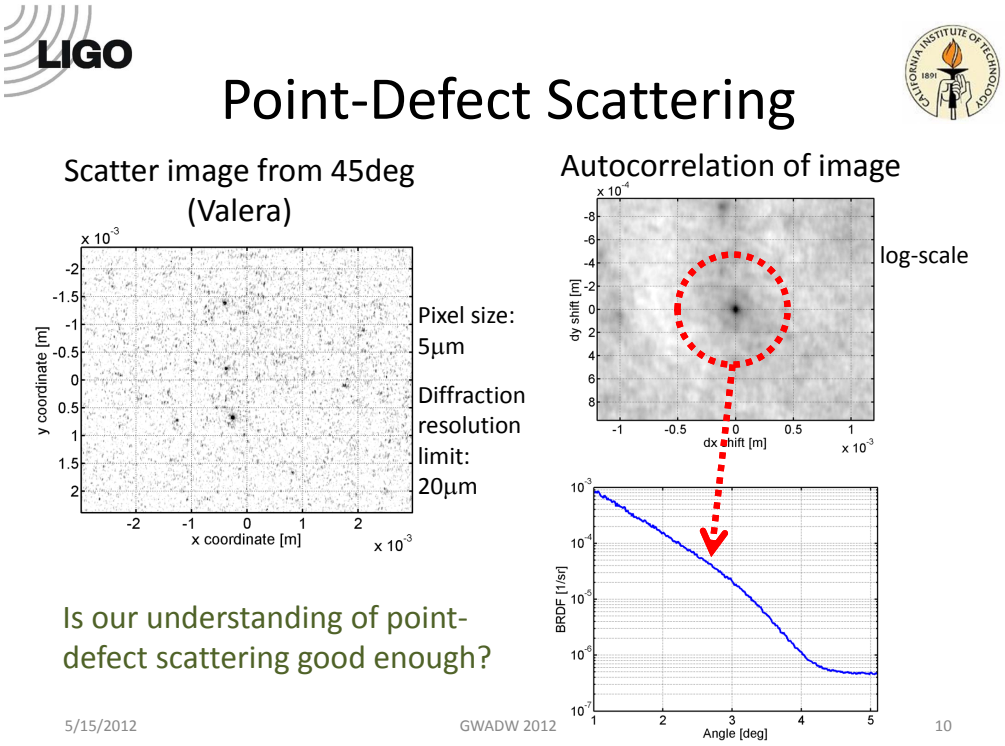

Figure 10: Slide taken from [13] showing an unexpected "bump" in measurements of BRDF performed on LIGO core mirrors. This seems to suggest that the model usually employed for predicting the BRDF from the mirror map could be too simplistic. The measured BRDF becomes flat for $\theta_s > 4°$, roughly in agreement with the value obtained from [2]

References

[1] W. Kells, C. Vorvick, "Imaged Scattered light from LIGO Resonant Cavities: Micro-roughness vs Point Scatter Loss", Ligo Internal Note, G080078-01-D (2008) 2

[2] Christopher J. Walsh, Achim J. Leistner, and Bozenko F. Oreb, "Power spectral density analysis of optical substrates for gravitational-wave interferometry", Applied Optics Vol. 38, No. 22, 1 August 1999 2, 12, 13, 14

[3] A. Chiummo for SLC, "Preliminary Computation of AdV arm-cavity baffle displacement noise projection" - Talk at GWADW2012, VIR-0188A-12 2, 3

[4] A.Chiummo, J.Marque, "Calculation of displacement noise induced by the cryotrap baffle", VIR-0272A-12 2, 3, 6, 7

[5] Jean-Yves Vinet, "Backscattering noise from cryotraps", VIR-0344A-10 2

[6] The Virgo collaboration, "Advanced Virgo Technical Design Report", VIR-0128A-12, and updates. 2

[7] R. Day, "A new FFT code: FOG Fast Fourier Transform Optical Simulation of Gravitational Wave Interferometers" - Talk at GWADW2012 3

[8] M. Evans, "Optickle, frequency domain Matlab methods for doing interferometer simulation". Optickle home-page 3

[9] Dainty C (Ed), Laser Speckle and Related Phenomena, 1984, Sprinter Verlag, ISBN 0-387-13169-8 5

[10] John C. Stover, "Optical Scattering: Measurement and Analysis", SPIE Press Monograph 1995 4, 12

[11] Michael Smith, "Wide Angle Scatter from ETM HR", LIGO- T1200425 6, 11

[12] E. Flanagan and K. Thorne, LIGO Technical note T940063-00-R 6, 11

[13] Jan Harms, "Scatter Loss in Quantum Noise Filter Cavities", talk at GWADW held on 14 May 2012, LIGO Document G1200634-v1. 12, 14